applied optics

Highly coherent supercontinuum generation in a photonic crystal fiber based on $GeSe_2$–As_2Se_3–PbSe chalcogenide in the mid-infrared region

Tham Tran Hong,[1] Thuan Nguyen Xuan,[1] Hue Thi Nguyen,[1] Van Thuy Hoang,[2] and Hieu Van Le[1,*]

[1]Faculty of Natural Sciences, Hong Duc University, 565 Quang Trung Street, Thanh Hoa City, Vietnam
[2]Department of Physics, Vinh University, 182 Le Duan, Vinh City, Vietnam
*Levanhieu@hdu.edu.vn

Received 21 February 2024; revised 12 June 2024; accepted 21 June 2024; posted 24 June 2024; published 11 July 2024

We numerically demonstrated highly coherent mid-infrared (IR) super-continuum (SC) generation using all-normal dispersion (AND) $GeSe_2$–As_2Se_3–PbSe chalcogenide photonic crystal fiber (PCF). The structural parameters of this PCF were optimized to obtain an ultra-flat-AND region and high nonlinearity characteristics using the full-vectorial finite difference method with the perfectly matched layer boundary conditions to calculate the linear properties of the fiber. We show that, pumping a light source at 9.8 μm pump wavelength with an input pulse energy of 3.5 nJ and pulse width of 200 fs, corresponding to the peak power of 17.5 kW, into a 10-cm-long fiber, an ultra-flat-coherent mid-IR SC extended from 2851.8 nm to 13538.8 nm (bandwidth of 10687 nm) is obtained. This ultra-wide and flattened spectrum has excellent stability and coherence properties that can be used for mid-IR applications such as biological imaging, optical coherence tomography, and frequency metrology.

https://doi.org/10.1364/AO.521750

1. INTRODUCTION

The mid-infrared (MIR) super-continuum (SC) source has developed as a groundbreaking advancement in optical technology in recent years due to its great potential in diverse fields such as infrared imaging [1], bio-photonic diagnostics [2], optical coherence tomography [3], and nonlinear MIR spectroscopy [4]. The MIR (typically from approximately 2.0 to 20.0 μm) is a unique electromagnetic spectral region because most molecules exhibit fundamental vibrational absorption bands in this region and leave distinctive spectral fingerprints [5]. SC generation involves the spectral broadening of short-duration and narrow-wavelength-band optical pulses to create broadband light sources [6]. Many applications require such lasers with specific properties such as extraordinary bandwidth, a high average power, and particular coherence properties. For example, optical coherence tomography requires an SC light source with low coherence [7], while laser synchronization, frequency metrology, and nonlinear microscopy applications require an extremely high coherent broadband spectrum [8–10]. Therefore, obtaining the SC spectrum in the MIR with controlled properties is very important and remains a challenge in the past few decades, rendering highly coherent MIR to be a well-established and matured technology.

It is possible to control the coherence characteristics of the generated SC spectra by tailoring the geometrical parameters of the fiber and pumping conditions, leading to a suitable spectral broadening mechanism [11]. Indeed, we can obtain highly coherent SC spectra by injecting femtosecond laser pulses into an optical fiber performing normal-dispersion region. In this case, the broadening of the SC spectrum is governed by the presence of the self-phase modulation (SPM) effect and the optical wave-breaking (OWB) effect. Due to these nonlinear effects, a deterministic phase relationship between the following generated wavelength and the initial pump pulse one is maintained, resulting in the elimination of noise-sensitive soliton dynamics and forming a highly coherent SC spectrum. Another commonly employed method for producing coherent and compressible SC spectra is the suppression of soliton fission in optical fibers with two closed zero-dispersion wavelengths (ZDWs) whose centers are near the pump wavelength. This phenomenon can cause a modulation instability contributing to an anomalous dispersion regime. Although we could not obtain the broadening spectrum with extremely high coherence, it was applied in coherent anti-Stokes Raman scattering microscopy successfully [12]. In some recent reports [13–15], authors proved that it is possible to eliminate modulation instability

effectively in involving nonlinear processes by reducing the distance between ZDW points, which, subsequently, generates highly coherent SC sources [15].

Up to now, a number of investigations in both theoretical and experimental studies on SC generation have been published by the researchers, in which a high coherence of SC generation in photonic crystal fibers (PCFs) in the mid-IR regime has been proposed. These short-length fibers can be made of a variety of materials, which allows us to use several different techniques to spontaneously obtain high nonlinearities and low dispersion properties. A typical proposed method is using highly nonlinear soft glass materials such as fluoride [16], tellurite [17], lead-bismuth-gallate [18,19], or chalcogenide glass [20]. Among others, the lead–bismuth–gallate glasses have higher mechanical durability and a very high nonlinear refractive index (10 times higher than that of silica). However, the attenuation of this compound-glass type is significantly larger than the attenuation of fused-silica fibers. Fluoride-made fibers are difficult to fabricate because of low thermal stability ($\Delta T = 60°C$) and steep viscosity characteristic curve around the fiber drawing temperature [16]. In fact, most fluoride fibers used for the generation of SC spectra in the MIR region are supplied by the commercial factory, which limits work on controlling the dispersion properties of the fiber. Tellurite glass introduces more thermal stability properties with $\Delta T \geq 100°C$ and a higher nonlinear refractive index in comparison to fluoride glass. This glass fiber type has a ZDW of around 2.0 μm [17]. However, both fluoride and tellurite glasses are well transparent only for wavelengths shorter than 5.5 μm and, thus, limit their usage for applications at longer wavelengths. Among these soft glasses, the most widely used material to make optical fibers to broaden SC spectra in the mid-IR is chalcogenide glass, which introduces a wider transmission range (over wavelengths of 20 μm). It also possesses higher nonlinearity compared with other soft glasses [17,19]. Due to the high nonlinearity properties, the fibers can create a broadband SC spectrum in the MIR region by using comparatively shorter fiber lengths and lower pump powers, making them more suitable as host materials for waveguide fabrication than most other materials. In addition, this type of glass can be resistant to recrystallization after multi-steps of thermal processes, which enables using stack-and-draw technique for optical fiber fabrication [21].

Many theoretical and experimental studies on using step-index fibers and PCFs made from chalcogenide glasses for SC generation have been conducted and obtain impressive results [22–25]. Xing *et al.* performed numerical simulations strongly supported by experimental results for observing SC spectra generation in chalcogenide fiber paths with lengths ranging from 0.34 to 10 cm. The results were obtained with pump wavelengths 2070–2080 nm lasing from a femtosecond fiber laser source. At a peak power of 2.9 kW, the generated supercontinuum spectrum had a bandwidth of 3 dB of 27.6 THz and a bandwidth of −20 dB of 75.5 THz [22]. A $Ga_8Sb_{32}S_{60}$ chalcogenide-based PCF has been studied for coherent SC generation in 1.0-cm-long fiber by using a pump laser pulse of 50 fs pulse width 20 kW peak power and at a wavelength of 4.5 μm [23]. A broad, flat-top, and highly coherent SC spectrum covering a wavelength range of 1.65–9.24 μm at the 20 dB spectral flatness was generated. Vyas *et al.* have fabricated a 6 μm core-diameter optical fiber made of Ge–Sb–Se/Ge–Se glasses, which had zero group velocity dispersion at two wavelengths of around 4.2 μm and around 7.3 μm [24]. Using the light source at a wavelength of 4.485 μm, 330 fs pulse width, to pump into a fiber with a length of 11.0 cm, the authors obtained the SC spectrum extending from the wavelength of 2.2 μm to 12 μm with an output average power of ∼17 mW. For step-index fiber based on chalcogenide (As_2Se_3), Cheng *et al.* reported the generation of broadband SC spanning from 2.0 to 15.1 μm using a pump at a wavelength of 9.8 μm with a peak power of 2.98 MW. Although this is the broadest MIR-SC generation observed so far in optical fibers, the peak power is very high, on the order of megawatts [25]. However, almost all fibers considered for SC generation have only flat-dispersion properties. Additionally, the metallic characteristic of composites forming the glass has the tendency of recrystallization or increasing absorption, which are also weak points of this material in the realization of the desired fibers. For instance, in the work of Zhang and his colleagues, an ultra-broadband SC spectrum (with a wavelength range of 1.7–12.7 μm) with high coherent properties was generated experimentally at a pump wavelength of 5.5 μm using 7.0-cm-long PCF fiber made from chalcogenides $Ge_{20}As_{20}Se_{15}Te_{45}$ and $Ge_{20}As_{20}Se_{20}Te_{40}$, having the normal-dispersion region [26]. However, the metallic characteristics of the Te chemical element can introduce a higher possibility of recrystallization, which can cause strong scattering, consequently leading to more losses. Besides that, such a metallic characteristic also caused a low bandgap that resulted in strong background carrier absorption at room temperature by thermally excited charge carriers. As an alternative solution, it is possible to alleviate those drawbacks by substituting a small amount of Te with Se. This method can reduce the conductivity and dramatically increase the resistance to crystallization while retaining a wide optical transmission range.

In our study, we have carried out a series of numerical simulations to study a photonic crystal fiber in a $GeSe_2-As_2Se_3-PbSe$ (GAP-Se) chalcogenide glass as a waveguide medium for highly coherent SC generation in the MIR region. The GAP-Se chalcogenide glass exhibits outstanding optical properties, including a high nonlinear refractive index $n_2 = 71.4 \times 10^{-20}\ m^2/W$ at $\lambda = 3.0\ \mu m$ [27] (around 32 times higher than that for fused silica $n_2 = 2.19 \times 10^{-20}\ m^2/W$ [28], also higher than the refractive index one for lead–bismuth–gallate glass $n_2 = 20 \times 10^{-20}\ m^2/W$ [19]). Moreover, this glass has a broad transmission window spanning from 1.0 to 12.0 μm [29], which is wider than that of other chalcogenide glasses (As_2S_5) [30]. In addition, this glass provides good rheological properties and relevant expansion coefficients as well as thermal matched coefficients [21]. Those points make the glasses good candidates for fabricated fiber structures with the optimization of the crystallization resistance as well as thermal stability after multistage thermal processes in the stack-and-draw method [21]. Aiming at an ultra-flat all-normal dispersion (AND) in the mid-IR region, the PCF cross section was specifically designed with optimized geometrical parameters including the lattice pitch (Λ) and air-hole diameter (d) in the cladding. Herewith, the generalized nonlinear Schrödinger equation (GNLSE) governing the optical pulse propagation in the proposed PCF is solved by theoretical calculations and numerical simulations.

The results are in good agreement such that we can generate a mid-IR SC spectrum with desired properties in the proposed PCF. In addition, the coherence of the generated SC spectra is also numerically investigated and discussed in detail.

2. DESIGN OF THE PHOTONIC CRYSTAL FIBER STRUCTURE

In this work, we designed a $GeSe_2-As_2Se_3-PbSe$ (GAP-Se) chalcogenide–glass PCF with a hexagonal structure cross section (schematically shown in Fig. 1) for waveguiding fundamental fiber mode and producing the highly coherent SC spectrum in the MIR wavelength region. The structural cross section of such an optical fiber consists of six air-hole rings in its cladding defined by the lattice pitch Λ and air-hole diameter d, which gives the filling factor as defined as the ratio of the air holes' diameter to the lattice pitch $f = d/\Lambda$. In particular, fibers are designed with different air-hole diameters, in which d_1, d_2, d_3, and d_4 present the diameter of the air holes in the first ring, the second ring, the third ring, and the remaining rings in the PCF cladding, respectively.

For all numerical simulations, we used the commercial software Lumerical MODE solutions with the full-vectorial finite difference method with the perfectly matched layer boundary conditions to calculate the dispersion properties of the fiber [31]. As aforementioned, the fiber is made of GAP-Se glass composition. This is because the material introduces a very high nonlinear refractive index profile and a wide transmission range.

The real linear refractive index of GAP-Se is fitted using the following Sellmeier equation, as below:

$$n = \sqrt{A + \frac{B_1\lambda^2}{\lambda^2 - C_1} + \frac{B_2\lambda^2}{\lambda^2 - C_2}}, \tag{1}$$

where $A = -20.6611$, $B_1 = 28.5635$, $B_2 = 10.4782$, $C_1 = 0.05345344\ \mu m^2$, and $C_2 = 8175.52322596\ \mu m^2$ are Sellmeier coefficients [27] and λ is the wavelength in micrometers.

Figure 2(b) shows the transmission spectrum of the GAP-Se at wavelengths up to 10 μm. This glass has a broad transparency window spanning from 1.0 to 20.0 μm, which is much wider than that of other chalcogenide glasses [30].

The chromatic dispersion profile is an important factor that determines of different spectral components of the ultra-short pulse propagating at different phase velocities through the fiber. The expression of chromatic dispersion to effective refractive index n_{eff} is given below [32]:

$$D(\lambda) = -\frac{\lambda}{c}\frac{d^2 n_{eff}}{d\lambda^2}, \tag{2}$$

where λ is the wavelength and c is the speed of light vacuum.

For the work involving SC generation processes in optical fibers and tailoring the properties of the generated SC spectra, in general, the initial and crucial condition is to have a low and ultra-flat normal-dispersion profile. Indeed, the low dispersion profile is needed to reduce the temporal widening of the

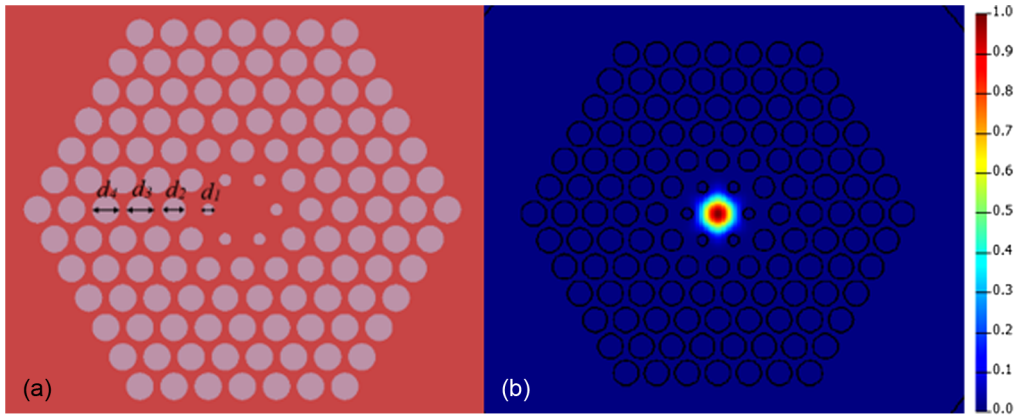

Fig. 1. (a) Schematic of the designed PCF structure and (b) intensity distribution of the fundamental mode.

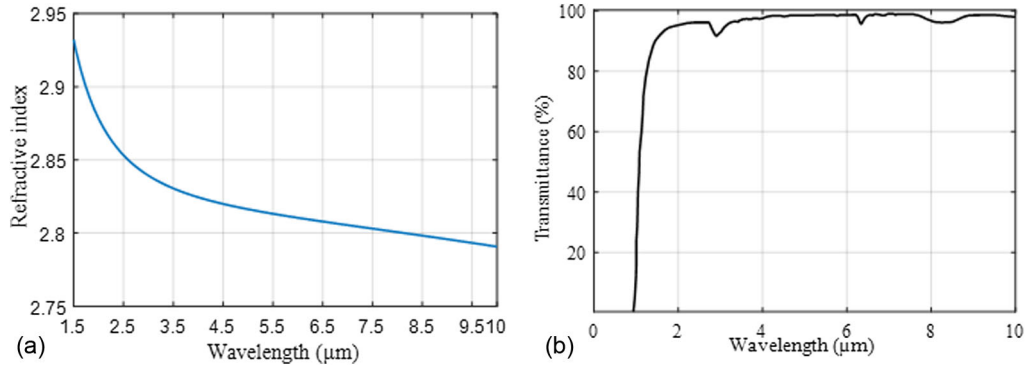

Fig. 2. (a) Refractive index of GAP-Se and (b) transmission spectrum of the GAP-Se [29].

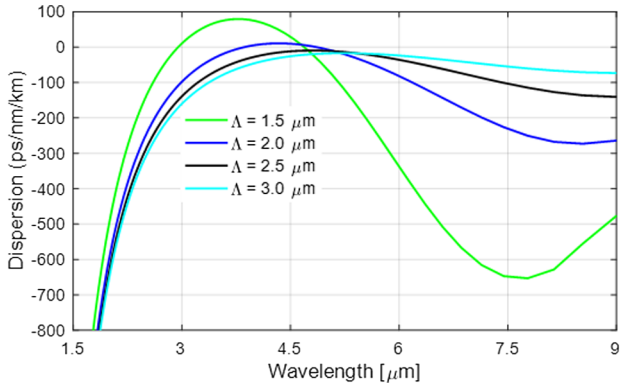

Fig. 3. Dispersion profiles of the fundament mode of the PCF with different lattice constants keeps the hole diameter at 1.0 μm.

pulse during propagation inside the fiber, allowing nonlinear phenomena such as SPM and OWB [33]. Meanwhile, the PCF having normal-dispersion characteristics results in good conditions supporting processes of broadening SC spectra with a high coherent property. The low noise sensitivity of the normal-dispersion profile helps to reduce the impact of noise and fluctuations on the input pulse, resulting in a smoother and more uniform spectral and temporal profile. Therefore, our aim is to design a GAP-Se PCF structure to obtain a low and ultra-flat all-normal dispersion in the MIR region. For this purpose, a number of simulations were carried out to optimize the geometrical parameters, i.e., lattice pitch and the diameters of air holes of the designed PCF. The possibility of controlling the Λ and d allows engineering the dispersion profile of the PCF in a wide wavelength range [34].

First, we studied the influence of the lattice constant on the properties of the fiber's dispersion in a wavelength range from 1.5 μm to 15.0 μm. In this step, lattice constant is varied between 1.0 and 3.0 μm with a step of 0.5 keeping the hole diameter at 1.0 μm as shown in Fig. 3. It can be seen that the designed PCF fiber exhibits both the normal and anomalous dispersion regions or all-normal-dispersion ranges. When increasing the lattice constant, the dispersion curve shifts from the anomalous to normal-dispersion region very rapidly, and the zero-dispersion wavelengths (ZDWs) shift towards the longer wavelength region. In the case of $\Lambda = 2.0$ μm, the dispersion of the used fiber becomes flat and reaches the lowest value in the both all-normal and anomalous regions. Thus, we selected this value of the lattice constant $\Lambda = 2.0$ μm for further analysis.

In the next investigations, numerical calculations were performed for a set of different diameter values of the air holes d_1, d_2, d_3, and d_4 in the cladding. The numerical results showed that changing the diameter d_1 of the first-round air holes introduces the biggest influence on the maximum-dispersion wavelength and the shape of the dispersion curve considered in the wavelength range longer than 3.0 μm. When we increased the diameter d_1, the dispersion shifted from the normal to the anomalous dispersion region, and the dispersion curve became less flattened as shown in Fig. 4(a).

In the case of changing the diameter d_2 of the second-round air hole, this not only changes the peak-dispersion point but also strongly affects the flatness of the dispersion characteristic, especially in the wavelength range from 3.5 μm to 8.0 μm [Fig. 4(b)]. As we increase the diameter d_2, the dispersion curve becomes flatter and gradually becomes monotonous. Moreover, the study also showed that there was almost no influence on

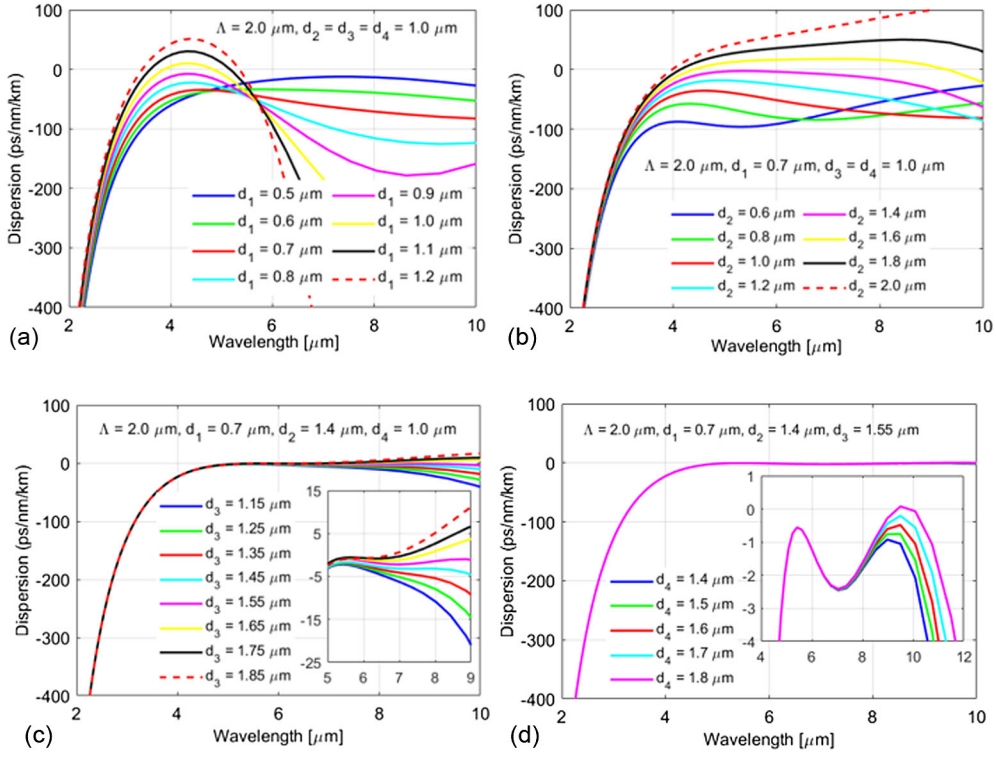

Fig. 4. Dispersion characteristics of the fundamental mode of the PCF. The fiber has a lattice constant $\Lambda = 2.0$ μm and different diameters of air holes.

the maximum-dispersion wavelength due to the change of the diameter d_3 and d_4 considered in the range of 7.0–10.0 μm [Figs. 4(c) and 4(d)]. However, increasing the diameter d_3 can make the dispersion flatter, and it eventually becomes monotonic in that wavelength range [Fig. 4(c)]. Meanwhile, changing the diameter d_4 can produce a small change in the flat of the dispersion properties [Fig. 4(d)]. In detail, increasing the diameter d_4 can shift the dispersion curve upward, especially in the wavelength range from 9.0 μm to 10.0 μm. Therefore, by controlling lattice constant and cladding air-hole diameters that correspond to different filling factors ($f = d/\Lambda$) of the fiber lattice, it is possible to precisely tailor the dispersion profile of the optical fiber. It also can be seen that we can obtain a significant change in dispersion properties of the fiber with a small adjustment of the air-hole diameters on the level of 0.1 μm.

To the end, based on these preliminary calculations, we obtained the PCF with optimized geometrical parameters given in Table 1. The proposed PCF introduces a dispersion profile with the lowest values and ultra-flatness properties in all-normal-dispersion regimes considered for the MIR region. That ultra-flattened normal dispersion varies from −2.441 to −0.544 ps/nm/km within a wavelength range from 4.81 μm to 10.68 μm (a bandwidth of 5870 nm) as depicted in Fig. 5. It can be seen that at the wavelength of 9.8 μm, the simulated chromatic dispersion of the proposed optical fiber receives a value of −0.55 ps/nm/km.

It should be noticed that the nonlinear coefficient is another important factor supporting the Kerr nonlinearity phenomenon in this optical fiber medium. This coefficient is proportional to the nonlinear refractive index n_2 and also inversely proportional to the effective-mode area of the considered fiber as in the following expression [32]:

Table 1. Lattice Pitch and Hole Diameter of the Proposed PCF Structure

Parameter	Value
Lattice pitch Λ [μm]	2.00
Hole diameter d_1 [μm]	0.70
Hole diameter d_2 [μm]	1.40
Hole diameter d_3 [μm]	1.55
Hole diameter d_4, d_5, d_6 [μm]	1.60

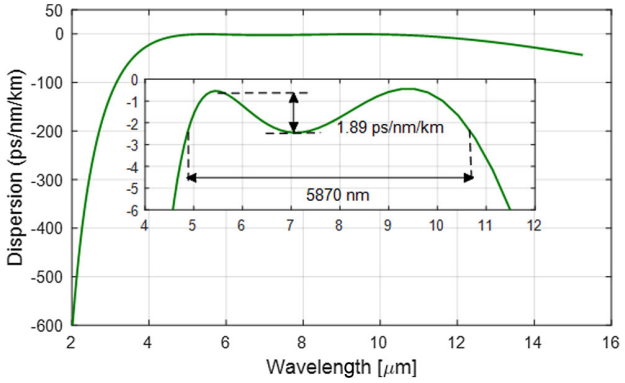

Fig. 5. Chromatic dispersion of the fundamental mode of the proposed PCF.

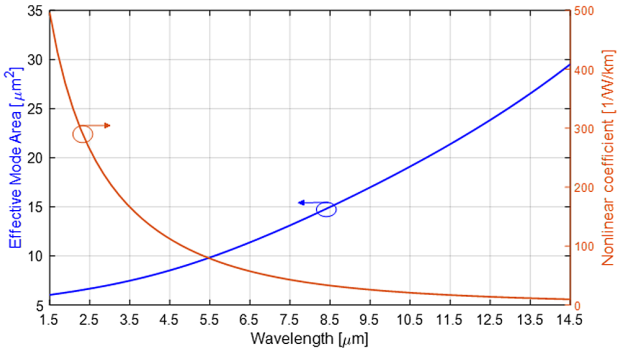

Fig. 6. Fundamental mode effective index and nonlinear coefficient of the proposed PCF.

$$\gamma(\lambda) = \frac{2\pi n_2}{\lambda A_{\text{eff}}}, \tag{3}$$

where $n_2 = 71.4 \times 10^{-20}\ \text{m}^2/\text{W}$ is the nonlinear refractive index of used GAP-Se glass [27], and A_{eff} represents the effective-mode area of the fiber, as given by the formula [32]

$$A_{\text{eff}} = \frac{\left(\iint |E|^2 \mathrm{d}x\mathrm{d}y\right)^2}{\iint |E|^4 \mathrm{d}x\mathrm{d}y}, \tag{4}$$

where $E(x, y)$ represents the field distribution of the fiber mode.

Figure 6 shows the effective-mode area and nonlinear coefficient of the fundamental mode propagating in the proposed fiber at different wavelengths. It can be seen that the effective-mode area of the fundamental mode increases almost linearly with respect to the wavelengths. Meanwhile, the proposed PCFs have large nonlinear coefficients. At the wavelength of 9.8 μm, the effective-mode area and nonlinear coefficient of fundamental mode of the proposed fiber are 17.39 μm^2 and 26.6 $\text{w}^{-1}\ \text{km}^{-1}$, respectively.

3. NUMERICAL ANALYSIS OF SC GENERATION IN THE DESIGNED PCF STRUCTURE

A. Numerical Modelling Method

In this section, the evolution of the light pulses along the longitudinal coordinate z of the considered fiber was simulated using the GNLSE in the frequency domain with noise present in the input pulses, as given by [32]

$$\frac{\partial A}{\partial z} + \frac{\alpha}{2}A + \sum_{n=2}^{\infty} i^{(n-1)} \frac{\beta_n \partial^n A}{n! \partial t^n} = i\gamma\left(1 + \frac{i}{\omega_0}\frac{\partial}{\partial t}\right) A(z, t)\left[\int_{-\infty}^{\infty} R(t')\left|A(z, (t-t')\right|^2 \mathrm{d}t'\right], \tag{5}$$

where α and β_n are the total loss and the nth order of dispersion of the considered PCF fiber, respectively.

In our model, we used the Gaussian pulse as input pulses, which is given as the formula

$$A(T) = \sqrt{P_0}\exp\left(\frac{-T^2}{2t_0^2}\right), \tag{6}$$

where A represents the longitudinal envelope of the pulse, and P_0 and t_0 are the peak power and pulse width of the input pulse.

The other nonlinear term in Eq. (5) represents the Raman response, which is mainly contributed by the electronic and vibrational factors. Assuming that the electronic factor is instantaneously contributed, the Raman response function R_t can be written as below [32]:

$$R(t) = (1 - f_R)\delta(t) + f_R h_R(t), \tag{7}$$

where $\delta(t)$ introduces the Dirac delta function. f_R is the fractional contribution of the delayed Raman response function $h_R(t)$, which has an approximate analytical form [32]:

$$h_R(t) = \frac{\tau_1^2 + \tau_2^2}{\tau_1 \tau_2^2} \exp(-t/\tau_2) \sin\left(-\frac{t}{\tau_1}\right) \Theta(t), \tag{8}$$

where $\Theta(t)$ is the Heaviside step function and $\tau_1 = 23.1$ fs and $\tau_2 = 195$ fs for GAP-Se glass [27].

Coherence is one of the important characteristics of a light source concerned in many applications. For example, in spectroscopy and some other quantitative techniques, the fluctuations in intensity may cause increasing the noise, which reduces the signal-to-noise ratio. For the SC spectrum generated in our proposed PCF, its coherence characteristic was influenced by the quantum noise of the input pulse. To study this event, we used one-photon-per-mode semi-classical theory [32], and the coherence degree is expressed in the following formula:

$$\left|g_{12}^{(1)}(\lambda, t_1 - t_2 = 0)\right| = \left|\frac{\langle E_1^*(\lambda, t_1) E_2(\lambda, t_2)\rangle}{\left[\langle |E_1(\lambda, t_1)|^2\rangle \langle |E_2(\lambda, t_2)|^2\rangle\right]^{1/2}}\right|, \tag{9}$$

where $E_1(\lambda)$ and $E_2(\lambda)$ are the amplitudes of the electric field of the generated spectra. The value of $g_{12}^{(1)}$ is in the range of [0,1], where $g_{12}^{(1)} = 1$ for high coherent spectrum, and $g_{12}^{(1)} = 0$ for incoherent light.

B. Numerical Analysis of SC Generation in the Proposed PCF Structure

In this section, the SC spectrum generated in the designed PCF was numerically studied using an input pulse with the following parameters: pump wavelength of 9.8 μm, pulse width of 200 fs, and peak power with several selected values. This input light pulse can be obtained experimentally using the Ti:sapphire mode-locked seed laser (Coherent Mira 900) and the difference frequency generation (DFG) as reported in [25]. However, in this work, we focus on the numerical analysis of super-continuum generation in the proposed PCF, so we would not detail the procedure of experimental generation of the pump source. With the target of seeking the optimal SC spectra with a large bandwidth and high coherent properties, we conducted a set of numerical simulations with the input peak powers being changed in a range of 0.05 kW to 20.0 kW and the step fixed at 0.01 nJ for input energy. In this work, due to the studied pump wavelength located in the normal-dispersion regime, the broadening spectrum phenomena are mainly governed by SPM and OWB effects [33]. The OWB effect contributes to both processes of leading and trailing edges of the pulse. This effect begins when spectral side lobes are generated due to mixing the overlapping frequency components which are actually formed by SPM effect. The SPM phenomenon then supports generating extreme wavelengths on both sides of the spectrum and contributing to the uniform temporal and spectral profiles for the final results of SC generation processes.

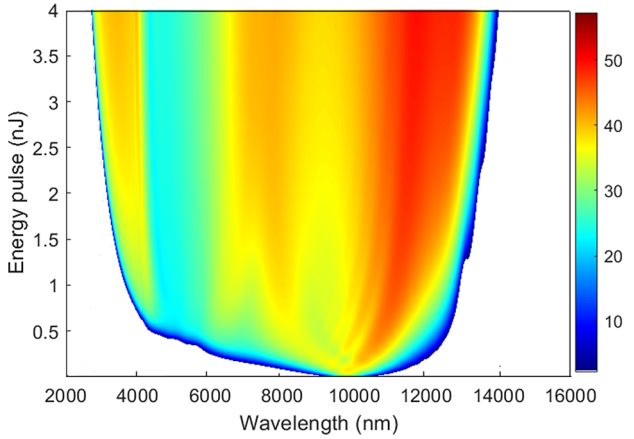

Fig. 7. Evolution of the broadened SC spectra as a function of input energy in a 10-cm-long proposed fiber at a pumping wavelength of 9.8 μm and pulse width of 200 fs.

The first set of numerical calculations in this task is to investigate the influence of the pulse energy on the bandwidth of the generated SC spectrum in a 10-cm-long fiber. The simulation results are presented in Fig. 7. Herewith, when we changed the pulse energy from 0.01 nJ to 4.0 nJ, the corresponding peak power changed from 0.05 kW to 20.0 kW. It can be seen that at lower values of the input energy (smaller than 0.3 nJ), there are broadening limitations, which are mainly caused by the SPM effect with the significant change in the group velocity dispersion in the visible compared to the mid-IR. On the other hand, for the higher level of the input pulse energy (higher than 0.3 nJ), there is the appearance of clear spectral broadening in which the spectral center was contributed by the SPM effect and OBW was responsible for broadening the spectral wings.

The next set of simulations was carried out to study the mid-IR spectral broadening with various peak power. The obtained results, depicted in Fig. 8(a), show that we obtained a wider bandwidth of the output SC spectrum by increasing the peak power of the pulse. For example, for a pulse peak power of 2.5 kW, we achieved the octave spanning of the SC spectrum in the MIR wavelength range of 4308.5–12290.3 nm. Meanwhile, with a peak power of 12.5 kW, a broad SC spectrum spanning from 3041.28 nm to 13152.8 nm was obtained. Besides that, we also checked the influence of the peak power on the coherence properties of the generated SC spectra. The studied results are shown in Fig. 8(b). It can be seen that the SC output with highly coherent properties expanded in longer wavelength ranges when increasing the input pulse peak power. As a result, in all cases considered in the teams of peak powers, the SC generation in the proposed PCF is fully coherent from the wavelength range of 4000 nm to 14000 nm since its value is approximately 1.

In another set of numerical calculations, we investigated the influence of the pulse widths on the SC spectrum generated in the same 10-cm-long fiber used in the previous simulation

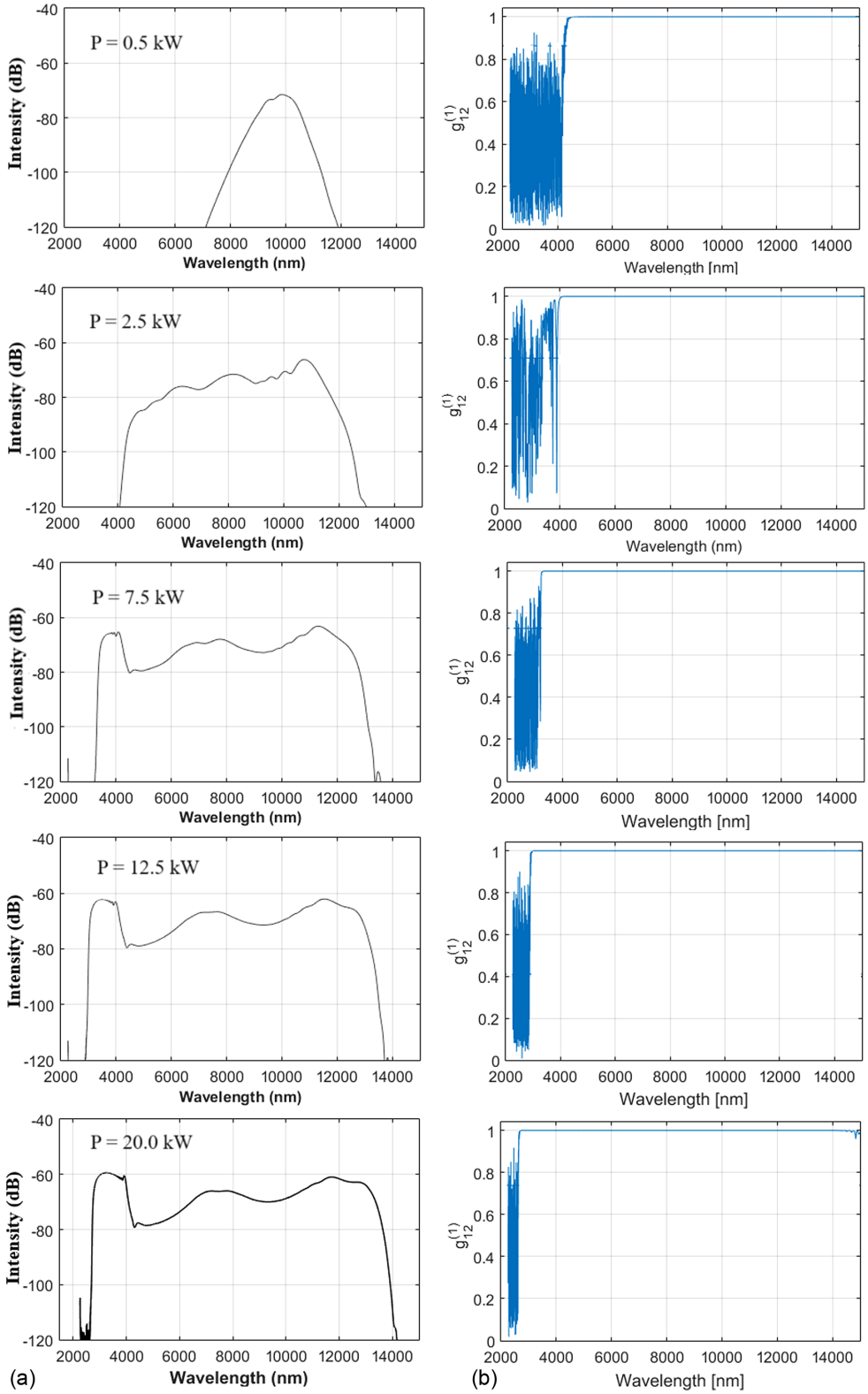

Fig. 8. (a) Simulated SC spectra at the output of 10-cm-long chalcogenide PCF and (b) coherence property of generated SC spectrum pumped at 9.8 μm laser pulse with various peak powers.

set. Figure 9 shows the spectral evolution, output spectrum, and coherence of optical pulses with the pump wavelength of 9.8 μm.

The obtained result demonstrates that the SC spectral bandwidth is almost dependent on the pulse widths, with the resulting super-continuum spectrum spanning from

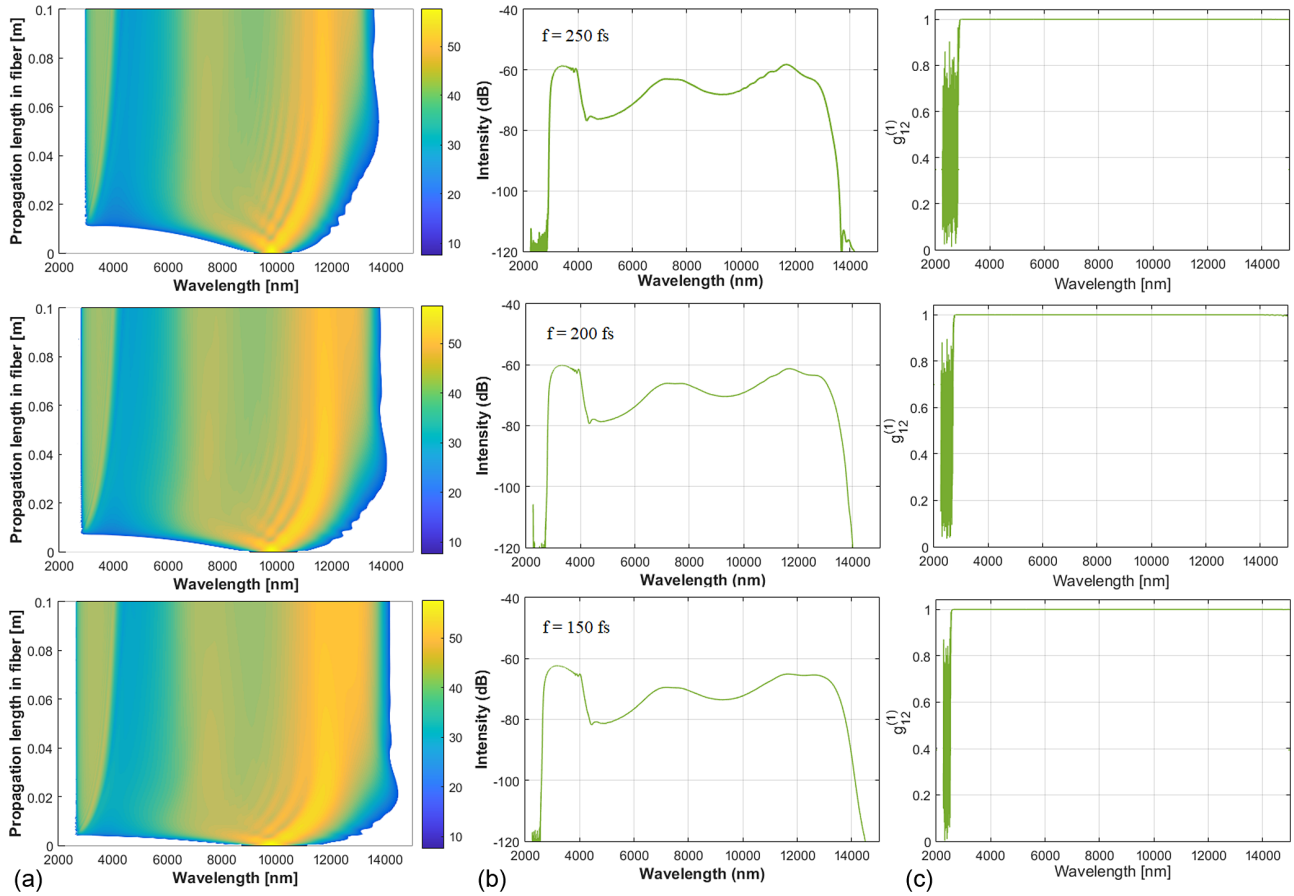

Fig. 9. (a) Spectral evolution, (b) output spectrum, (c) and coherence characteristics of optical pulses with pump wavelength of 9.8 μm in a fiber length of 10 cm.

9926.78 nm to 10764.8 nm in all considered cases as shown in Fig. 9(b). In addition, decreasing pulse widths leads to a substantial increase in the bandwidth of SC spectra output and enhances its flatness. For example, for a pulse width of 250 fs, the octave spanning of the SC spectrum was achieved in the mid-IR wavelength range of 3055.22 nm to 12982 nm, while in the case of pulse width with 150 fs, broad SC spectra spanning the mid-IR region and extending from 2714.98 nm to 13569.5 nm can be achieved. In addition, in these cases, the AND PCF pumped with laser pulses, the nonlinear coupling between nonlinear effects contributes to the suppression of incoherent dynamics, and, as a result, a highly coherent SC spectrum is obtained [35], as shown in Fig. 9(c).

To the end, we numerically performed SC generation in our 10-cm-long proposed fiber for the selected case with an input pulse energy of 3.5 nJ and a pulse width of 200 fs, corresponding to the peak power of 17.5 kW. As a result, we obtained a highly coherent SC spectrum in the MIR region with a bandwidth of 10687 nm ranging from the wavelength of 2851.8 nm to 13538.8 nm within 18.3 dB dynamics as depicted in Fig. 10(a). This bandwidth is reduced from 10687 to 9671 nm ($\Delta B = 1016$ nm) if the air holes in the third, fourth, fifth, and sixth cladding rings of the fiber design have the same diameter of 1.55 μm.

Meanwhile, Fig. 10(b) represents the formation of the SC spectrum and its temporal profile along the propagation lengths. The SC generation occurs along the GAP-Se chalcogenide glass fiber with the support of SPM and OWB nonlinear effects. At the beginning path of the fiber, the SPM effect is responsible for the broadening mechanism of the spectrum with the S-shape temporal spectrogram, but with a clear asymmetry toward the blue side of the spectrum. In the following path of the fiber, OWB and higher-order dispersion are the dominant factors leading to blue and red shifts of the generated spectrum. One can see how the SC spectrum generated in the proposed fiber extends much further to the mid-IR wavelengths as the result of both a higher nonlinear refractive index and a lower dispersion value. Notice that the spectrum extending toward shorter wavelengths shows a significant reduction of the power spectral density, which is below that value for the pump pulse. After approximately 0.01 cm of propagation length, the energy is suddenly transferred to a wavelength band around 4200 nm with further propagation and is therefore responsible for the two-peaked structure and the depleted central part of the spectra generated in the all-normal-dispersion region. After a propagation length of 0.035 cm, the influence of the OWB effect becomes stronger and leads to the formation of side lobes on both sides of the generated spectrum [Fig. 10(b)]. In this work, both SPM and OWB effects play essential roles in broadening

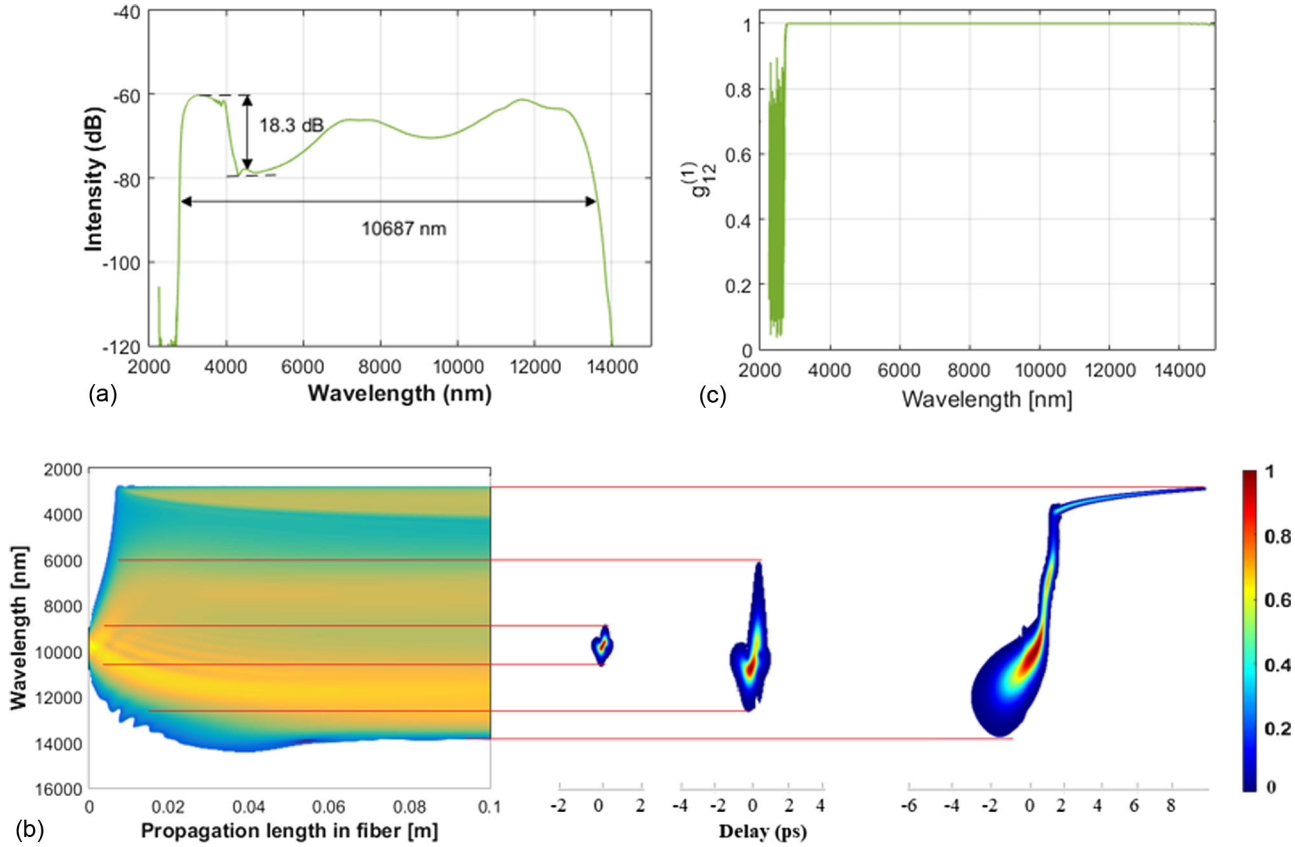

Fig. 10. (a) Output spectrum in 10 cm fiber length, (b) spectral evolution at various positions along propagation length, (c) and first-order coherence of optical pulses with the pump wavelength of 9.8 μm, 200 fs pulse width, and 3.5 nJ energy, corresponding to 17.5 kW in a 10 cm fiber length.

the SC spectrum. In these nonlinear processes, new components of the wavelengths with a phase related to the input pulse are generated, and the noise-sensitive soliton dynamics are suppressed [25]. Therefore, the SC spectrum maintains its coherence characteristic in the PCF having a normal-dispersion profile. It can be seen in Fig. 10(c) that the complex degree of the coherence factor is almost unity (which introduces a high coherence) in the whole considered wavelength range of SC generation.

In reality, in addition to the influence of quantum noise, the coherence property is also influenced by the noise of the input pulse, including polarization noise and pulse-to-pulse relative intensity noise. However, in the case of using short fiber lengths and short-duration pulses, the polarization noise may only have a small effect on the coherence property of the SC spectrum [36]. Therefore, in the last step, to investigate the coherence of the SC spectrum in the proposed PCF, we add the effects of the pulse-to-pulse relative intensity noise, which is the amplitude fluctuation of each input pulse, which also leads to fluctuations in the pulse duration, calculated by the formula $\delta t_0 = -0.8 \times (\delta A_{AN} - 1)$, where δt_0 is the pulse duration fluctuation, and δA_{AN} is a single random value. The mean of δA_{AN} is equal to 1, and its root-mean-square (rms) is provided by the manufacturer of the lasers. Here we examine the rms of the input laser whose value varies from 0.2% to 1% with a step of 0.2. The obtained results are depicted in Fig. 11. The coherence would further decrease if the RIN is taken into account. Its value

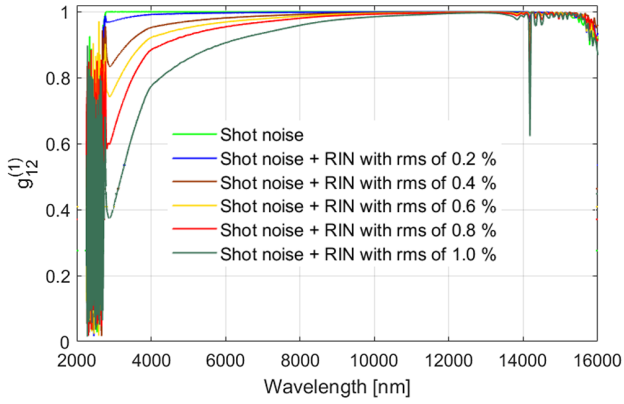

Fig. 11. Effect of shot noise and RIN noise with various values of root-mean-square of the laser with 9.8 μm pump wavelength, 200 fs pulse width, and 3.5 nJ energy, corresponding to 17.5 kW in a 10 cm fiber length.

is approximately 1 for the case of shot noise, while in the case of 0.2%, 0.4%, 0.6%, 0.8%, and 1.0%, the RIN has values below 0.98, 0.95, 0.85, and 0.8, respectively.

To highlight the results we obtained in this work, we represent an overview of SC generation in soft glass fibers as shown in Table 2. The proposed PCF offered the SC generation with a much larger spectral bandwidth in comparison with those obtained in the other fibers using the same input peak power [23,30,38,40] or using a smaller input peak power than that

Table 2. Bandwidth and Flatness of the SC Spectrum Generated in the Proposed GAP-Se Chalcogenide Glass PCF Compared with Several Fibers Made of Other Soft Glass in All-Normal-Dispersion Region

Soft Glass	Normal Dispersion	Fiber Length	Pump Wavelength (μm)	Peak Power (kW)	Spectral Flatness Level (dB)	Spectral Bandwidth (μm)	Refs.
$Ga_8Sb_{32}S_{60}$ chalcogenide	All-normal	1 cm	4.5	20	20 dB	1.65–9.24	[23]
As_2S_5 chalcogenide	All-normal	3.4 cm	5.3	10	30 dB	2.0–10.0	[30]
$(Ge_{10}Te_{43})_{90}-AgI_{10}$ Telluride	All-normal	14 cm	7.0	19 MW	40 dB	2.0–16.0	[35]
$Ge_{20}As_{20}Se_{15}Te_{45}$ chalcogenide	All-normal	7.0 cm	5.5	126 MW	—	2.2–11.1	[26]
As_2S_5 chalcogenide	All-normal	2.8 cm	10	1.3 MW	40 dB	2.0–14.0	[37]
Ge-As-Se chalcogenide	All-normal	—	4	16.5	10 dB	3.0–6.0	[38]
Tellurite	All-normal	—	3.5	50	>10 dB	1.1–4.6	[39]
$As_{40}Se_{60}$ chalcogenide	All-normal	2 cm	6.3	5	20 dB	3.3–8.5	[40]
$GeSe_2-As_2Se_3-PbSe$ chalcogenide	All-normal	10 cm	9.8	17.5	18.3 dB	2.81518–13.5388	This work

reported in [26,39]. Although the spectral bandwidth in our investigation is smaller than those achieved in [25,35,37], especially in [25], with step-index fiber made of the same material and the same input pump wavelength as in our study, we used a peak power much smaller than the ones used in those cases (about 1000 times smaller). This is an important advantage because using the low input peak power can reduce fiber damage involved in the thermal impact of the laser pulse.

4. CONCLUSION

We have demonstrated the numerical generation of a desired coherent SC spectrum in the MIR regime using our proposed photonic crystal fiber made of $GeSe_2-As_2Se_3-PbSe$ (GAP-Se) chalcogenide glass. Studying the geometrical parameters of the fiber including the lattice constant and diameter of the cladding air holes allowed us to obtain the optimized PCF with $\Lambda = 2.0$ μm and $d_1 = 0.7$ μm, $d_2 = 1.40$ μm, $d_3 = 1.55$ μm, and $d_4 = 1.6$ μm for high-coherent SC generation. This proposed PCF introduced an ultra-flat all-normal dispersion in the MIR region within a range of wavelengths from 4810 nm to 10680 nm (bandwidth of 5870 nm).

Our simulations have shown that we numerically obtained a highly coherent SC generation with an 18.3 dB spectral flatness for the very wide bandwidth of 10687 nm ranging from 2851.8 nm to 13538.8 nm when injecting an optical pulse at the wavelength of 9.8 μm with an energy of 3.5 nJ and a width of 200 fs, corresponding to the peak power of 17.5 kW into 10 cm length of the proposed fiber. Due to the great properties of the dispersion profile and the ability to generate desired highly coherent MIR SC spectra, the proposed GAP-Se chalcogenide–glass PCF design is expected to have potential applications in various fields including gas detection, inspecting food quality, metrology, high-spatial-resolution imaging, and mid-IR spectroscopy.

Disclosures. The authors declare no conflicts of interest.

Data availability. Data underlying the results presented in this paper are not publicly available at this time but may be obtained from the authors upon reasonable request.

REFERENCES

1. M. Verdonck, A. Denayer, B. Delvaux, *et al.*, "Characterization of human breast cancer tissues by infrared imaging," Analyst **141**, 606–619 (2016).
2. A. Labruyere, A. Tonello, V. Couderc, *et al.*, "Compact supercontinuum sources and their biomedical applications," Opt. Fiber Technol. **18**, 375–378 (2012).
3. X. Shu, M. Bondu, B. Dong, *et al.*, "Single all-fiber-based nanosecond-pulsed supercontinuum source for multispectral photoacoustic microscopy and optical coherence tomography," Opt. Lett. **41**, 2743–2746 (2016).
4. R. Su, M. Kirillin, E. W. Chang, *et al.*, "Perspectives of mid-infrared optical coherence tomography for inspection and micrometrology of industrial ceramics," Opt. Express **22**, 15804–15819 (2014).
5. S. Dai, Y. Wang, X. Peng, *et al.*, "A review of mid-infrared supercontinuum generation in chalcogenide glass fibers," Appl. Sci. **8**, 707 (2018).
6. C. Lafforgue, M. Montesinos-Ballester, T. T. D. Dinh, *et al.*, "Supercontinuum generation in silicon photonics platforms," Photon. Res. **10**, A43–A56 (2022).
7. I. Hartl, X. D. Li, C. Chudoba, *et al.*, "Ultrahigh-resolution optical coherence tomography using continuum generation in an air–silica microstructure optical fiber," Opt. Lett. **26**, 608–610 (2001).
8. J. Rothhardt, A. M. Heidt, S. Hädrich, *et al.*, "High stability soliton frequency-shifting mechanisms for laser synchronization applications," J. Opt. Soc. Am. B **29**, 1257–1262 (2012).
9. T. Udem, R. Holzwarth, and T. W. Hänsch, "Optical frequency metrology," Nature **416**, 233–237 (2002).
10. H. N. Paulsen, K. M. Hilligse, J. Thøgersen, *et al.*, "Coherent anti-stokes Raman scattering microscopy with a photonic crystal fiber based light source," Opt. Lett. **28**, 1123–1125 (2003).
11. K. L. Corwin, N. R. Newbury, J. M. Dudley, *et al.*, "Fundamental amplitude noise limitations to supercontinuum spectra generated in a microstructured fiber," Appl. Phys. B **77**, 269–277 (2003).
12. E. R. Andresen, H. N. Paulsen, V. Birkedal, *et al.*, "Broadband multiplex coherent anti-stokes Raman scattering microscopy employing photonic-crystal fibers," J. Opt. Soc. Am. B **22**, 1934–1938 (2005).
13. K. M. Hilligsøe, T. V. Andersen, H. N. Paulsen, *et al.*, "Supercontinuum generation in a photonic crystal fiber with two zero dispersion wavelengths," Opt. Express **12**, 1045–1054 (2004).
14. P. Falk, M. H. Frosz, and O. Bang, "Supercontinuum generation in a photonic crystal fiber with two zero-dispersion wavelengths tapered to normal dispersion at all wavelengths," Opt. Express **13**, 7535–7540 (2005).
15. A. Boucon, T. Sylvestre, K. P. Huy, *et al.*, "Supercontinuum generation by nanosecond dual-pumping near the two zero-dispersion wavelengths of a photonic crystal fiber," Opt. Commun. **284**, 467–470 (2011).

16. G. Qin, X. Yan, C. Kito, *et al.*, "Ultrabroadband supercontinuum generation from ultraviolet to 6.28 μm in a fluoride fiber," Appl. Phys. Lett. **95**, 161103 (2009).
17. P. Domachuk, N. A. Wolchover, M. Cronin-Golomb, *et al.*, "Over 4000 nm bandwidth of mid-IR supercontinuum generation in sub-centimeter segments of highly nonlinear tellurite PCFs," Opt. Express **16**, 7161–7168 (2008).
18. R. Buczynski, H. Bookey, M. Klimczak, *et al.*, "Two octaves supercontinuum generation in lead-bismuth glass based photonic crystal fiber," Materials **7**, 4658–4668 (2014).
19. H. Van Le, V. T. Hoang, G. Stepniewski, *et al.*, "Low pump power coherent supercontinuum generation in heavy metal oxide solid-core photonic crystal fiber infiltrated with carbon tetrachloride covering 930–2500 nm," Opt. Express **29**, 39586–39601 (2021).
20. C. R. Petersen, N. Prtljaga, M. Farries, *et al.*, "Mid-infrared multispectral tissue imaging using a chalcogenide fiber supercontinuum source," Opt. Lett. **43**, 999–1002 (2018).
21. M. Klimczak, B. Siwicki, A. Heidt, *et al.*, "Coherent supercontinuum generation in soft glass photonic crystal fibers," Photon. Res. **5**, 710–727 (2017).
22. S. Xing, S. Kharitonov, J. Hu, *et al.*, "Linearly chirped mid-infrared supercontinuum in all-normal-dispersion chalcogenide photonic crystal fibers," Opt. Express **26**, 19627–19636 (2018).
23. A. Medjouri, D. Abed, and Z. Becer, "Numerical investigation of a broadband coherent supercontinuum generation in $Ga_8Sb_{32}S_{60}$ chalcogenide photonic crystal fiber with all-normal dispersion," Opto-Electron. Rev. **27**, 1–9 (2019).
24. S. Vyas, T. Tanabe, M. Tiwari, *et al.*, "Chalcogenide photonic crystal fiber for ultraflat M-IR supercontinuum generation," Chin. Opt. Lett. **14**, 123201 (2016).
25. T. Cheng, K. Nagasaka, T. H. Tuan, *et al.*, "Mid-infrared supercontinuum generation spanning 2.0 to 15.1 μm in a chalcogenide step-index fiber," Opt. Lett. **41**, 2117–2120 (2016).
26. N. Zhang, X. Peng, Y. Wang, *et al.*, "Ultrabroadband and coherent mid-infrared supercontinuum generation in Te-based chalcogenide tapered fiber with all-normal dispersion," Opt. Express **27**, 10311–10319 (2019).
27. P. Chauhan, A. Kumar, and Y. Kalra, "Numerical exploration of coherent supercontinuum generation in multicomponent $GeSe_2$-As_2Se_3-PbSe chalcogenide based photonic crystal fiber," Opt. Fiber Technol. **54**, 102100 (2020).
28. H. L. Van, V. T. Hoang, T. Le Canh, *et al.*, "Silica-based photonic crystal fiber infiltrated with 1,2-dibromoethane for supercontinuum generation," Appl. Opt. **60**, 7268–7278 (2021).
29. C. Goncalves, M. Kang, B. U. Sohn, *et al.*, "New candidate multicomponent chalcogenide glasses for supercontinuum generation," Appl. Sci. **8**, 2082 (2018).
30. H. T. Tong, A. Koumura, A. Nakatani, *et al.*, "Chalcogenide all-solid hybrid microstructured optical fiber with polarization maintaining properties and its mid-infrared supercontinuum generation," Opt. Express **30**, 25433–25449 (2022).
31. Lumerical Solutions, Inc., http://www.lumerical.com/tcad-products/mode/.
32. G. Agrawal, *Nonlinear Fiber Optics*, 6th ed. (Academic, 2019).
33. J. M. Dudley and J. R. Taylor, *Supercontinuum Generation in Optical Fibers* (Cambridge University, 2010).
34. H. V. Le, V. L. Cao, H. T. Nguyen, *et al.*, "Application of ethanol infiltration for ultra-flattened normal dispersion in fused silica photonic crystal fibers," Laser Phys. **28**, 115106 (2018).
35. Z. Zhao, B. Wu, X. Wang, *et al.*, "Mid-infrared supercontinuum covering 2.0–16 μm in a low-loss telluride single-mode fiber," Laser Photon. Rev. **11**, 1700005 (2017).
36. I. Kubat and O. Bang, "Multimode supercontinuum generation in chalcogenide glass fibres," Opt. Express **24**, 2513–2526 (2016).
37. K. Nagasaka, L. Liu, T. H. Tuan, *et al.*, "Supercontinuum generation in chalcogenide double-clad fiber with near zero-flattened normal dispersion profile," J. Opt. **19**, 095502 (2017).
38. M. Meneghetti, X. Forestier, C. R. Petersen, *et al.*, "Graded index chalcogenide fibers with nanostructured core," Adv. Photon. Res. **2**, 2000091 (2021).
39. T. K. Phan, L. D. Vu, H. P. T. Nguyen, *et al.*, "Coherent mid-infrared supercontinuum generation in tellurite all-solid microstructured optical fibers with anomalous and normal dispersion property," Results Opt. **13**, 100576 (2023).
40. B. Siwicki, A. Filipkowski, R. Kasztelanic, *et al.*, "Nanostructured graded-index core chalcogenide fiber with all-normal dispersion–design and nonlinear simulations," Opt. Express **25**, 12984–12998 (2017).